Fluorine 18 Fluorodeoxyglucose PET/CT Volume-based Indices in Locally Advanced Non–Small Cell Lung Cancer: Prediction of Residual Viable Tumor after Induction Chemotherapy[1]

Michael Soussan, MD
Joanna Cyrta, MD
Christelle Pouliquen, MD
Kader Chouahnia, MD
Fanny Orlhac, MS
Emmanuel Martinod, MD, PhD
Véronique Eder, MD, PhD
Jean-François Morère, MD, PhD
Irène Buvat, PhD

Purpose: To study whether volume-based indices of fluorine 18 fluorodeoxyglucose positron emission tomographic (PET)/computed tomographic (CT) imaging is an accurate tool to predict the amount of residual viable tumor after induction chemotherapy in patients with locally advanced non–small cell lung cancer (NSCLC).

Materials and Methods: This study was approved by institutional review board with waivers of informed consent. Twenty-two patients with locally advanced NSCLC underwent surgery after induction chemotherapy. All had pre- and posttreatment FDG PET/CT scans. CT largest diameter, CT volume, maximum standardized uptake value (SUV_{max}), mean SUV (SUV_{mean}), metabolic tumor volume (TV), and total lesion glycolysis of primary tumor were calculated. Changes in tumor measurements were determined by dividing follow-up by baseline measurement (ratio index). Amounts of residual viable tumor, necrosis, fibrous tissue, inflammatory infiltrate, and Ki-67 proliferative index were estimated on resected tumor. Correlations between imaging indices and histologic parameters were estimated by using Spearman correlation coefficients or Mann-Whitney tests.

Results: No baseline or posttreatment indices correlated with percentage of residual viable tumor. TV ratio was the only index that correlated with percentage of residual viable tumor (r = 0.61 [95% confidence interval: 0.24, 0.81]; P = .003). Conversely, SUV_{max} and SUV_{mean} ratios were only indices correlated with Ki-67 (r = 0.62 [95% confidence interval: 0.24, 0.82]; P = .003; and r = 0.60 [95% confidence interval: 0.21, 0.81]; P = .004, respectively). Total lesion glycolysis ratio was moderately correlated with residual viable tumor (r = 0.53 [95% confidence interval: 0.13, 0.78]; P = .01) and with Ki-67 (r = 0.57 [95% confidence interval: 0.18, 0.80]; P = .006). No ratios were correlated with presence of inflammatory infiltrate or foamy macrophages.

Conclusion: TV and total lesion glycolysis ratios were the only indices correlated with residual viable tumor after induction chemotherapy in locally advanced NSCLC.

[1] From the Departments of Nuclear Medicine (M.S., V.E.), Pathology (J.C., C.P.), Oncology (K.C., J.F.M.), and Thoracic Surgery (E.M.), AP-HP, Avicenne Hospital, 125 rue de Stalingrad, 93000 Bobigny, France; and IMNC-UMR 8165 CNRS-Universités Paris 7 and 11, Orsay, France (M.S., F.O.); and CEA-SHFJ, Orsay, France (I.B.). Received September 18, 2013; revision requested October 23; revision received January 20, 2014; accepted February 11; final version accepted February 25. **Address correspondence to** M.S. (e-mail: *michael.soussan@avc.aphp.fr*).

Lung cancer is one of the most frequent malignant tumors and represents the leading cause of death by cancer in Europe and in the United States (1,2). Surgery is the treatment of choice in early-stage non–small cell lung cancer (NSCLC). The treatment of locally advanced NSCLC has evolved during the past 2 decades, and the current standard of care is combined-modality therapy, including chemotherapy, radiation therapy, and surgery (3). Induction chemotherapy followed by surgery has been used in stage III cancer to address the high rate of local and systemic failure (4). Induction treatment before surgery can produce a tumor downstaging that increases the likelihood of complete resection, organ preservation, and long-term survival. Therefore, an accurate prediction of tumoral response after induction chemotherapy in stage III NSCLC is crucial to determine which patients will benefit from surgery.

Several studies (5,6) have suggested that the degree of residual viable tumor after induction therapy, determined by histopathologic findings in the resected tumor, may be a more objective criterion of chemotherapy response than imaging criteria. The most recent study showed that the percentage of residual viable tumor cells helps predict overall and disease-free survival in patients with resected NSCLC after induction chemotherapy even when controlled for pathologic stage (7).

Metabolic imaging with fluorine 18 fluorodeoxyglucose (FDG) positron emission tomography (PET) is increasingly used for prediction of histologic response after chemotherapy. Despite existing guidelines (8,9), there is an ongoing debate about the parameters that should be measured to assess therapeutic response. Positive correlations between standardized uptake value (SUV) changes during treatment and histopathologic regression have been observed in NSCLC (10–13). However, studies about accuracy of PET for prediction of histologic response after induction treatment in NSCLC have yielded contradictory results (14,15). Scanning protocols, SUV measurement, and best cutoff values were not standardized, and a sound meta-analysis is difficult (10–13). Maximum SUV (SUV_{max}), which is used in most studies, depends on several acquisition and processing parameters and does not reflect the spatial distribution of the tracer within the lesion. Our assumption was that measurement methods that accounted for the metabolically active tumor volume might add relevant information regarding residual tumor cells (16,17). Our purpose was to study whether volume-based parameters could bring additional information compared with SUV measurements to predict the residual viable tumor seen at histologic analysis after induction treatment in patients with NSCLC.

Advances in Knowledge

- Volume-based index changes on fluorine 18 fluorodeoxyglucose (FDG) PET/CT scans between baseline scan and after induction chemotherapy scan are the only parameters correlated with the amount of residual viable tumor after induction chemotherapy in locally advanced non–small cell lung cancer (NSCLC) (tumor volume [TV]: $r = 0.61$ [95% confidence interval: 0.24, 0.81]; $P = .003$; total lesion glycolysis: $r = 0.53$ [95% confidence interval: 0.13, 0.78] $P = .01$).
- Maximum standardized uptake value (SUV) and mean SUV ratios between the two scans were correlated with Ki-67 proliferative index after induction chemotherapy ($r = 0.62$; $P = .003$; and $r = 0.60$; $P = .004$, respectively).

Implication for Patient Care

- Volume-based indices (TV and total lesion glycolysis ratios) on FDG PET/CT scans help predict residual viable tumor after preoperative chemotherapy in locally advanced NSCLC and might help identify patients who will benefit from the surgery.

Materials and Methods

Patients and Induction Chemotherapy

This study was approved by our institutional review board with waivers of informed consent. Between January 2009 and June 2011, 34 consecutive patients with potentially resectable biopsy-proved stage III NSCLC were treated with induction chemotherapy and underwent FDG PET/computed tomographic (CT) imaging before and after the induction treatment. In addition to FDG PET/CT, initial routine staging procedures consisted of a clinical examination, including lung function tests, bronchoscopy and/or mediastinoscopy, thoracic enhanced CT, and brain imaging, by using enhanced CT or magnetic resonance imaging. Disease had been staged according to the seventh edition of the International Union Against Cancer TNM classification (18). Operability was assessed by the performance status, lung function status, and cardiac status of the patient. Induction treatment was composed of three cycles of

Published online before print
10.1148/radiol.14132191 **Content code:** CH

Radiology 2014; 272:875–884

Abbreviations:
FDG = fluorine 18 fluorodeoxyglucose
NSCLC = non–small cell lung cancer
RECIST = Response Evaluation Criteria In Solid Tumors
SUV = standardized uptake value
SUV_{max} = maximum SUV
SUV_{mean} = mean SUV
TV = tumor volume

Author contributions:
Guarantors of integrity of entire study, M.S., K.C., V.E., I.B.; study concepts/study design or data acquisition or data analysis/interpretation, all authors; manuscript drafting or manuscript revision for important intellectual content, all authors; approval of final version of submitted manuscript, all authors; literature research, M.S., J.C., K.C., E.M., V.E., I.B.; clinical studies, M.S., K.C., E.M., V.E., J.F.M., I.B.; experimental studies, J.C., C.P., K.C., I.B.; statistical analysis, M.S., K.C., F.O., J.F.M., I.B.; and manuscript editing, M.S., J.C., C.P., K.C., J.F.M., I.B.

Conflicts of interest are listed at the end of this article.

a platinum-based chemotherapy given every 3 weeks. Staging was repeated after completion of induction chemotherapy, including thoracic enhanced CT and FDG PET/CT. Patients with tumoral and/or mediastinal node downstaging according to Response Evaluation Criteria In Solid Tumors (RECIST) 1.1 criteria underwent surgery (22 of 34 patients). These 22 patients were the population study. Patients without mediastinal node downstaging or with a progressive disease underwent a thoracic radiation therapy with or without chemotherapy.

Patient age and sex, histologic subtypes, type of chemotherapy, and type of surgery are presented in Table 1. The study population consisted mostly of men (15 of 22 patients), and 14 of the patients had stage IIIA N2 disease. Six patients had stage IIIB (TNM stage T4N2M0) and two patients had stage IIIA non-N2 disease. The histopathologic subtypes were squamous cell carcinoma (11 patients), adenocarcinoma (eight patients), and large cell carcinoma (three patients). After the course of the platinum-based induction chemotherapy, all patients underwent surgical treatment: 16 patients underwent lobectomy, four underwent pneumonectomy, and two underwent bilobectomy. All patients had a complete resection of the primary tumor with negative margins and complete thoracic lymphadenectomy. Five of the 22 patients had N2 disease according to postsurgical histologic analysis, and they underwent subsequent mediastinal radiation therapy.

Histologic Assessment

All slides (107 slides) stained with hematoxylin-eosin safran were available for the 22 patients, and initial pathologic reports were retrieved from the archives. At least one section per 1 cm of tumor had been obtained during sampling. In cases with no residual carcinoma, the entire tumoral mass was submitted. Gross pathologic reports were reviewed to ensure that no necrotic or fibrotic core had been left unsampled. The following general characteristics of the tumor were noted: size (based on gross pathologic analysis), tumor stage (18), and presence or absence of nodal involvement. The number of slides examined per case ranged from three to 11 (median, five slides). All slides were scanned at magnification of ×400 through a high-resolution digital slide scanner (NanoZoomer 2.0 HT; Hamamatsu Photonics KK, Hamamatsu City, Japan), and two pathologists (J.C., C.P.) who were blinded to clinical and radiologic findings independently reviewed the results using viewer software (NDP; Hamamatsu Photonics KK).

For each slide, the zone that contained the tumor and/or evidence of tumor regression was the zone of interest, and its area was measured. In this zone, the percentage of each of the following items was assessed: *(a)* remaining viable tumor cells, *(b)* necrosis, and *(c)* fibrous tissue (including fibrous stroma, scar fibrosis, and elastosic replacement) (Fig 1). A weighted average of each of these values was calculated for all slides, where the weight for each slide was equal to the tumor area in the slide so that a percentage of viable tumor, necrosis, and fibrous tissue cells was determined for each tumor. The inflammatory infiltrate (composed of lymphocytes and/or neutrophils) and the presence of foamy macrophages were both assessed by using a binary semiquantitative scale (sparse or moderate and abundant) (Fig 1). In case of discrepancy (≥10% or one point of intensity), slides were reviewed simultaneously by both pathologists, and consensus was obtained.

Ki-67 proliferative index immunostaining for each tumor was obtained on the part with highest tumor cellularity by using a mouse monoclonal antibody (MIB-1; DAKO, Carpinteria, Calif; dilution 1:50) and a staining platform (Ventana BenchMark XT; Ventana Medical Systems, Tucson, Ariz). Any intensity of brown nuclear staining was considered to indicate positivity. Proliferative index percentage was assessed for 1000 cells of the most proliferative area at magnification of ×400 (19).

Table 1

Patient Characteristics

Variable	Result
No. of men	15
No. of women	7
Median age (y)	61 (50–80)
Clinical stage	
IIIA N2	14
IIIB (T4N2)	6
IIIA non-N2 (T3N1)	2
Induction chemotherapy	
Cisplatin + gemcitabin*	16
Carboplatin + paclitaxel†	3
Carboplatin + pemetrexed‡	3
Median time from postchemotherapy PET to surgery (wk)	8 (3.4–11.8)
Type of surgery	
Lobectomy	16
Pneumonectomy	4
Bilobectomy	2
Histologic type	
Squamous cell carcinoma	11
Adenocarcinoma	8
Large cell carcinoma	3
Median tumor size (cm)	4.9 (1.4–12)
Histologic analysis after chemotherapy (median)	
Residual viable tumor cells (%)	45 (0–79)
Necrosis (%)	8 (0–47)
Fibrous tissue (%)	40 (10–100)
Inflammatory infiltrate (no.)	
Sparse	11
Moderate to abundant	11
Foamy macrophages (no.)	
Absent or sparse	17
Moderate to abundant	5
Median proliferative index Ki-67	61 (0–94)

Note.—Unless otherwise indicated, data are the number of patients; data in parentheses are range.

* Cisplatin (25 mg/m^2 administered every 21 days on days 1, 2, 3, and 4) with gemcitabin (1 g/m^2 administered every 21 days on days 1 and 8).

† Carboplatin (dose corresponding to an area under the concentration-time curve of 6 mg/mL · min; administered every 21 days on day 1) with paclitaxel (175 mg/m^2 administered every 21 days on day 1).

‡ Carboplatin (dose corresponding to an area under the concentration-time curve of 5 mg/mL · min; administered every 21 days on day 1) with pemetrexed (500 mg/m^2 administered every 21 days on day 1).

Figure 1

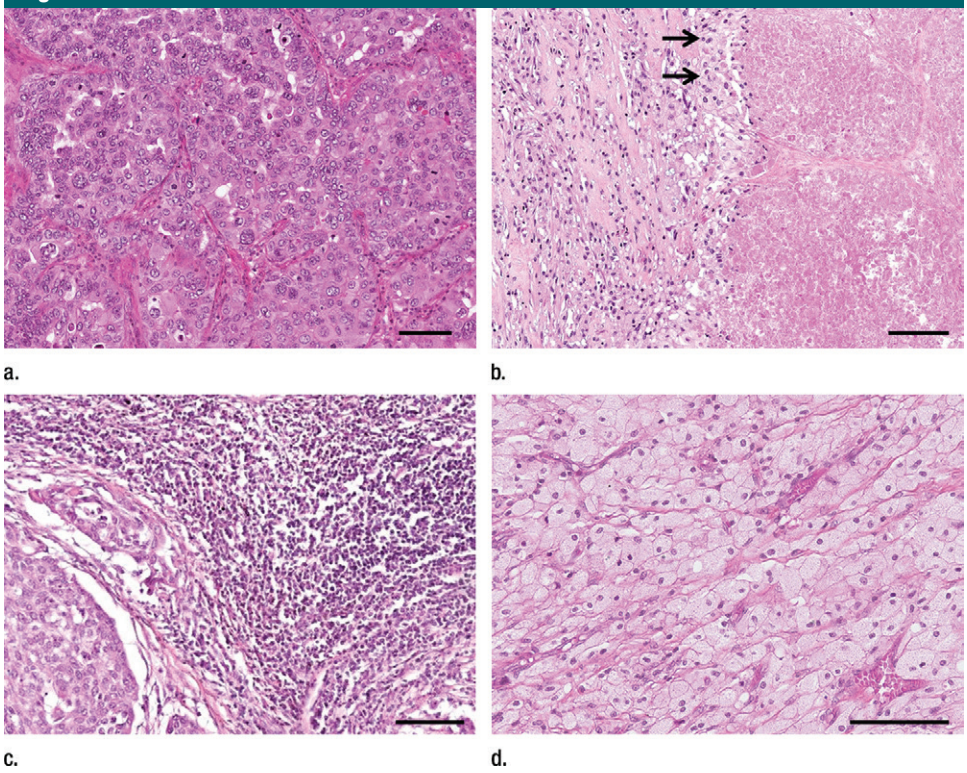

Figure 1: Exemplary photomicrographs of histopathologic analysis (hematoxylin-eosin stain; scale bar, 100 μm). **(a)** Nests of viable tumor cells (adenocarcinoma). **(b)** Necrosis (right) surrounded by a rim of foamy macrophages (arrows) and fibrous tissue (left). **(c)** Inflammatory infiltrate (lymphocytes) surround residual tumor cells (bottom left). **(d)** Confluent sheets of foamy macrophages in a complete responder.

FDG PET/CT Protocol

Baseline FDG PET/CT imaging was performed within 1 month of the start of chemotherapy. Follow-up FDG PET/CT imaging was performed in all patients approximately 2 weeks after administration of the last dose of the chemotherapy. PET/CT imaging was performed 60 minutes after intravenous injection of 3 MBq/kg of FDG. Serum glucose level was less than 1.4 g/L at the time of injection for all patients. All FDG PET/CT images were obtained by using a PET/CT scanner (Gemini TF; Philips Medical Systems, Best, the Netherlands) (20,21). Time per bed position was 105 seconds. CT images were obtained without injection of contrast media by using the following settings: 120 kV; 100 mA; collimation, 16 × 1.5 mm; pitch, 0.69; section thickness, 3 mm; increment, 1.5 mm. PET images were reconstructed by using a blob ordered subset–time of flight list-mode iterative algorithm with two iterations and 33 subsets, including attenuation and scatter corrections. A single-scatter simulation model was used for scatter correction (22). No postreconstruction smoothing filter was used. The image voxel size was 4 × 4 × 4 mm for PET and 1.17 × 1.17 × 1.5 mm for CT. SUVs were calculated from the reconstructed activity concentration values and were normalized to body weight.

Image Analysis

PET/CT and enhanced CT scans were used to characterize lung primary tumor and mediastinal nodes before and after induction chemotherapy (M.S., 10 years of experience). The largest diameter of the primary tumor (ie, the CT diameter) was measured from a single enhanced CT transverse image described in the RECIST 1.1 guidelines (23). The CT volume of each primary tumor was computed by using a commercially available lung analysis software package (CT Oncology Engine; Siemens, Forchheim, Germany) (17,24). On PET images, each primary lung tumor was automatically outlined by using the fit method described by Tylski et al (25). SUV_{max} and mean SUV (SUV_{mean}) were then calculated, which resulted in the tumor volume (TV). SUV_{mean} was intrinsically corrected for partial volume effect because the sampling and resolution effects were modeled in the tumor volume estimation method (25). Total lesion glycolysis was also calculated by using the following equation: total lesion glycolysis = $SUV_{mean} \times TV$. Changes in the primary tumor features were calculated by using index ratios that were obtained by dividing the follow-up by the baseline measurement. Index ratios that corresponded to changes in

CT size, SUV_{max}, SUV_{mean}, TV, and total lesion glycolysis were obtained for each lesion. Measurements were performed by using software (Planet Onco; Dosisoft, Cachan, France).

Statistical Analysis

Spearman rank correlation coefficients or Mann-Whitney tests were calculated to characterize the association between imaging parameters and histologic parameters.

Associated *P* values and 95% confidence intervals were calculated. Considering the sample size ($n = 22$) as well as an expected correlation coefficient set to 0.5, 95% confidence intervals around the correlation coefficient could be estimated with a precision around 0.3. The power of these analyses is greater than 0.8 when the correlation coefficient is greater than 0.5.

Despite the low number of patients, multivariate linear regressions were performed to provide head-to-head comparison between TV ratio and SUV_{max} ratio. Because total lesion glycolysis is calculated from SUV_{mean}, head-to-head comparison between total lesion glycolysis with SUV_{max} was not possible. The objective was to study whether the TV ratio was an independent predictor after adjustment for the effect of SUV_{max}. The normality hypothesis of TV and SUV_{max} needed for the linear regression analysis was successfully tested with Kolmogorov tests.

Because statistical analysis involved 108 correlations and associated tests (18 regressor criteria and six dependent variables), analyses were conducted in a stepwise manner to control a family-wise error rate of 5%.

Analyses were performed by using statistical software (R statistical software version 2.15.2, R Foundation for Statistical Computing, Vienna, Austria; and SAS version 9.1, SAS Institute, Cary, NC).

Results

Imaging Results

Imaging results of CT and PET before and after induction chemotherapy are described in Table 2. Results showed that the median ratios of CT volume, TV, and total lesion glycolysis were all below 0.5, whereas the median ratios of CT diameter and SUV indices were above 0.57.

Table 2

Values and Ratios in Primary Tumor Measurements on CT and PET Scans before and after Induction Chemotherapy

Parameter	Before Treatment	After Treatment	Ratio
CT diameter (mm)	48.5 (14–120)	38.3 (0–80)	0.7 (0–1)
CT volume (mL)	128 (1–400)	34 (0–154)	0.4 (0–0.9)
SUV_{max}	14.6 (2.4–19.7)	8 (0–25)	0.57 (0–1.6)
SUV_{mean}	8.9 (1.7–12)	4.6 (0–13)	0.58 (0–1.7)
TV (mL)	33 (1.6–190)	9.7 (0–53)	0.33 (0–1)
TLG (mL)	306 (3–1839)	37.6 (0–634)	0.21 (0–1.7)

Note.—Data are median and data in parentheses are range. TLG = total lesion glycolysis.

Histologic Results of the Primary Tumor

Histologic characterizations of the primary tumors are shown in Table 1. Two complete responses were observed, both in squamous cell carcinoma. The proportion of residual tumor cells in other cases ranged from 13% to 79% (median, 45%). Median proportions of necrosis and fibrosis were 8% (range, 0%–47%) and 40% (range, 10%–100%), respectively. Moderate to abundant inflammatory infiltrate was found in 11 cases (50%). Moderate to abundant foamy macrophages were seen in five cases (23%).

In 15 of 22 patients, the following features specifically associated with therapy-induced regression were observed: foam-cell rim surrounding necrosis, vascular granulation tissue adjoining scarred fibrosis, cholesterol clefts, and/or multinucleated giant cells (5,6).

Residual viable tumor and proliferation index were moderately correlated ($r = 0.49$; $P = .02$). Residual viable tumor and proliferative index Ki-67 were negatively correlated with the amount of fibrous tissue ($r = -0.9$; $P < .001$; and $r = -0.51$; $P = .02$, respectively).

Correlation between Imaging Indices and Histologic Analysis

The results of the correlation between CT and PET indices and histologic analysis of the primary tumor are summarized in Tables 3 and 4.

CT and PET indices before induction chemotherapy.—None of the baseline indices was correlated with the percentage of residual tumor cells. Large tumors characterized with a large diameter or volume at CT imaging before treatment exhibited more necrosis according to histologic analysis (Table 3). Large tumors characterized with a large CT diameter, CT volume, TV, and total lesion glycolysis were associated with a significant infiltrate of foamy macrophages ($P < .05$) (Table 4).

CT and PET indices after induction chemotherapy.—After induction chemotherapy, large tumors that were characterized by large CT diameter, CT volume, and TV exhibited more necrosis at histologic analysis (Table 3). SUV indices after treatment were positively correlated with a high proliferative index ($r = 0.49$; $P < .05$) and the presence of necrosis ($r = 0.63$; $P < .005$), but also negatively correlated with the amount of fibrous tissue ($r = -0.46$; $P < .05$). Large tumors characterized with a high CT diameter were associated with a significant infiltrate of foamy macrophages.

PET index ratios.—TV ratio was the only index that correlated with the percentage of residual viable tumor ($r = 0.61$ [95% confidence interval: 0.24, 0.81]; $P = .003$) (Table 3, Fig 2). SUV_{max} and SUV_{mean} ratios were moderately correlated with the percentage of residual viable tumor, but these correlations were not significant ($r = 0.38$ [95% confidence interval: −0.06, 0.68];

Table 3

Comparison of CT and PET Indices with Histologic Analysis of the Entire Primary Lung Tumor after Induction Chemotherapy

Parameter	Residual Viable Tumor (ρ)	Proliferative Index (ρ)	Necrosis (ρ)	Fibrous Tissue (ρ)
Before treatment				
CT diameter (mm)	0.10 (.66)	0.04 (.87)	0.56 (.007†)	−0.26 (.24)
CT volume (mL)	0.01 (.93)	0.07 (.76)	0.43 (.04†)	−0.15 (.49)
SUV_{max}	0.04 (.85)	−0.23 (.32)	0.25 (.26)	−0.08 (.74)
SUV_{mean}	0.01 (.98)	−0.24 (.28)	0.10 (.65)	0.02 (.93)
TV (mL)	0.01 (.95)	−0.01 (.95)	0.43 (.05†)	−0.19 (.39)
TLG (mL)	−0.03 (.90)	−0.07 (.77)	0.35 (.11)	−0.12 (.58)
After treatment				
CT diameter (mm)	0.14 (.54)	0.12 (.61)	0.59 (.004†)	−0.31 (.15)
CT volume (mL)	0.14 (.54)	0.16 (.5)	0.96 (.004†)	−0.33 (.13)
SUV_{max}	0.27 (.22)	0.49 (.02†)	0.68 (<.001†)	−0.47 (.003†)
SUV_{mean}	0.27 (.22)	0.50 (.02†)	0.63 (.002†)	−0.46 (.03†)
TV (mL)	0.27 (.22)	0.26 (.25)	0.65 (.001†)	−0.44 (.04†)
TLG (mL)	0.24 (.28)	0.34 (.13)	0.69 (<.001†)	−0.43 (.05†)
Ratios				
CT diameter ratio	0.30 (.17)	0.22 (.34)	0.11 (.63)	−0.25 (.26)
CT volume ratio	0.29 (.19)	0.15 (.5)	0.29 (.18)	−0.26 (.23)
SUV_{max} ratio	0.38 (.08)	0.62 (.003*)	0.44 (.04†)	−0.45 (.04†)
SUV_{mean} ratio	0.37 (.09)	0.60 (.004*)	0.42 (.05)	−0.43 (.05†)
TV ratio	0.61 (.003*)	0.32 (.16)	0.16 (.5)	−0.44 (.04†)
TLG ratio	0.53 (.01*)	0.57 (.006*)	0.34 (.12)	−0.54 (.01†)

Note.—Data in parentheses are *P* values. TLG = total lesion glycolysis.

* Statistically significant according to the stepwise analysis.

† $P < .05$ as exploratory analysis.

$P = .08$; and $r = 0.37$ [95% confidence interval: −0.07, 0.68]; $P = .09$, respectively). A multivariate regression model of the percentage of residual viable tumor, including TV ratio and SUV_{max} ratio, demonstrated that TV ratio was an independent predictive parameter after adjusting for the effect of SUV_{max}, but the reverse was not true. In this model, TV ratio significantly correlated with the percentage of residual viable tumor ($P = .05$), unlike SUV_{max} ($P = .61$).

SUV_{max} and SUV_{mean} ratios were correlated with Ki-67 proliferative index ($r = 0.62$ [95% confidence interval: 0.24, 0.82]; $P = .003$; and $r = 0.60$ [95% confidence interval: 0.21, 0.81]; $P = .004$, respectively) (Table 3, Fig 2). Total lesion glycolysis ratio was moderately correlated with the percentage of residual viable tumor ($r = 0.53$ [95% confidence interval: 0.13, 0.78]; $P = .01$) and with Ki-67 proliferative index ($r = 0.57$ [95% confidence interval: 0.18, 0.80]; $P = .006$). An illustration of a mismatch between TV and SUV_{max} ratios is shown in Figure 3.

CT volume ratios were neither correlated with the amount of residual viable tumor nor with the proliferative index Ki-67 (Table 3). None of the ratios was correlated with the presence of inflammatory infiltrate or foamy macrophages (Table 4).

Discussion

In this study, we evaluated the value of metabolic volumetric indices for prediction of the amount of residual viable tumor after induction chemotherapy in NSCLC. The residual viable tumor is the most validated histologic criteria for prognosis in patients with resected NSCLC after induction chemotherapy (5–7). Posttherapeutic SUV measurements did not accurately predict pathologic response to induction chemotherapy in NSCLC (14). Our results showed that metabolic volumetric (TV and total lesion glycolysis) changes under treatment of the primary tumor were the only factors positively correlated with the amount of residual tumoral cells after induction chemotherapy. Regarding FDG uptake, SUV ratios were positively correlated to proliferative index Ki-67. These results suggested that SUV changes under treatment reflected residual tumor proliferation, whereas volumetric changes reflected posttherapeutic viable cellular pool. PET volumetric indices might have the ability to reflect changes of the whole tumor mass, unlike SUV indices. Strength of this study was the thorough tumor sampling and analysis of all available slides to reliably determine the amount of residual tumor cells. Evaluation of only one section of the tumor, even the most representative, could bias the interpretation of correlation of imaging and histologic data (26). Moreover, all slides were digitized and reviewed by two pathologists to minimize the intra and inter observer variability.

In this study, tumor reduction assessed by metabolic volume changes was more accurate than that obtained by using changes in conventional indices, such as SUVs, CT diameter, or CT volume. Our results are in line with a recent report on breast tumor under induction treatment, where authors suggested that total lesion glycolysis changes predicted histopathologic tumor response with higher accuracy than did measurements of changes in SUV (27). Similarly, volumetric changes under treatment measured in FDG PET images could be more reliable than SUV changes in terms of survival in stage III–IV NSCLC factors (17,28).

TV and total lesion glycolysis, as defined in our study, can be computed easily and rapidly by using a semiautomatic adaptive threshold method with minimal interobserver variability. The segmentation method used here yields accurate tumor volume and SUV estimates (25). This method assumed that

Table 4

Comparison of CT and PET Indices with Degree of Inflammatory Infiltrate and Foamy Macrophages on Histologic Analysis of Entire Primary Lung Tumor after Treatment

	Inflammatory Infiltrate			Presence of Foamy Macrophages		
Parameter	Sparse	Moderate/Abundant	*P* Value	Sparse	Moderate/Abundant	*P* Value
Before treatment						
CT diameter (mm)	40 (16–83)	55 (14–120)	.11	44.5 (14–100)	83 (80–120)	.003*
CT volume (mL)	141 (1–400)	115 (1.41–296)	.50	69 (1.4–250)	281 (270–400)	.001*
SUV_{max}	13.7 (2.4–19.3)	14.7 (9.1–19.7)	.34	14.6 (4.5–19.3)	18.5 (9.1–19.7)	.28
SUV_{mean}	9 (1.7–12)	8.8 (5–11.8)	.62	8.9 (2.7–12)	11 (5–11.8)	.32
TV (mL)	27.4 (1.9–190)	33 (1.6–154)	.49	29.3 (1.6–190)	130 (98–154)	.006*
TLG (mL)	294 (3–1839)	317 (9–1699)	.45	285 (5.5–1839)	1150 (553–1699)	.01*
After treatment						
CT diameter (mm)	27 (0–62)	40 (8–80)	.49	26.5 (0–62)	62 (37–80)	.04*
CT volume (mL)	37 (0–153)	32 (0.4–122)	.90	27 (0–62)	62 (37–72)	.04*
SUV_{max}	7.3 (0–24.8)	8.3 (1–13.8)	.92	7.5 (0–24.8)	11.4 (4.1–16.4)	.25
SUV_{mean}	3.9 (0–13)	4.9 (0–7.8)	.92	4.2 (0–13)	5.4 (2.2–10)	.32
TV (mL)	6.3 (0–53)	10.4 (0–45)	.82	7.1 (0–52.8)	21 (16–51)	.06
TLG (mL)	19.6 (0–634)	39 (0–243)	.92	30 (0–634)	164 (36–505)	.08
Ratios						
CT diameter ratio	0.8 (0–1)	0.57 (0.46–0.88)	.08	0.71 (0–1)	0.67 (0.46–0.76)	.34
CT volume ratio	0.82 (0–0.96)	0.57 (0.46–0.88)	.09	0.49 (0–0.86)	0.15 (0.007–0.38)	.04*
SUV_{max} ratio	0.65 (0–1.6)	0.55 (0.1–1.25)	.38	0.54 (0–1.63)	0.66 (0.21–1.32)	.39
SUV_{mean} ratio	0.7 (0–1.7)	0.53 (0–0.97)	.28	0.54 (0–1.67)	0.66 (0.20–1.31)	.51
TV ratio	0.47 (0–1)	0.27 (0–0.46)	.05*	0.34 (0–1)	0.22 (0.11–0.39)	.25
TLG ratio	0.34 (0–1.7)	0.14 (0–0.30)	.06	0.24 (0–1.67)	0.14 (0.02–0.51)	.87

Note.—Data are median and data in parentheses are range. TLG = total lesion glycolysis.

* $P < .05$ as exploratory analysis.

the tumor image could be modeled as the convolution of the actual tumor volume of uniform activity with a three-dimensional Gaussian function that described the local spatial resolution in the reconstructed image. Despite the high degree of necrosis observed in some tumors after treatment (median, 8%; range, 0%–47%), we did not observe substantial hypometabolic tumoral area with visual analysis, and that could bias the results of the segmentation method. Furthermore, the fit method used in this study led to SUVs that were intrinsically corrected for partial volume effect (25). Partial volume effect can severely bias SUV estimates, especially in lesions that are small in size (ie, lesions that are less than three times the full width at half maximum of the reconstructed image resolution) (29). In our study, we observed strong changes in metabolic volumes before and after treatment, which suggested that these volumes were differently affected by partial volume effect. Intrinsic partial volume effect correction used in this study could have helped to reduce the effect of the partial volume effect confounding factor, which would highlight the correlation between posttherapeutic SUV_{mean} or SUV_{mean} ratios and the Ki-67 proliferative index.

Figure 2

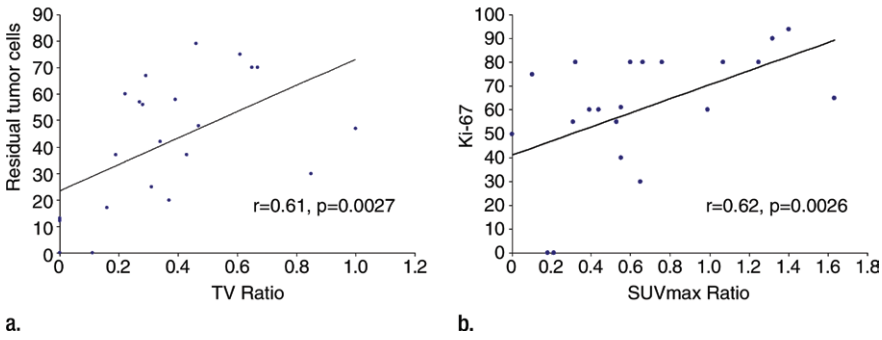

Figure 2: Graphs show **(a)** correlation between the TV ratio and residual tumor cells after induction chemotherapy and **(b)** correlation between the SUV_{max} ratio and proliferative index Ki-67 after induction chemotherapy. Residual tumor cells and proliferative index are expressed in percentages.

Previous studies regarding FDG uptake changes after induction treatment in NSCLC showed contradictory results. On the one hand, a reduction in SUV_{max} tends to be greater in complete

Figure 3

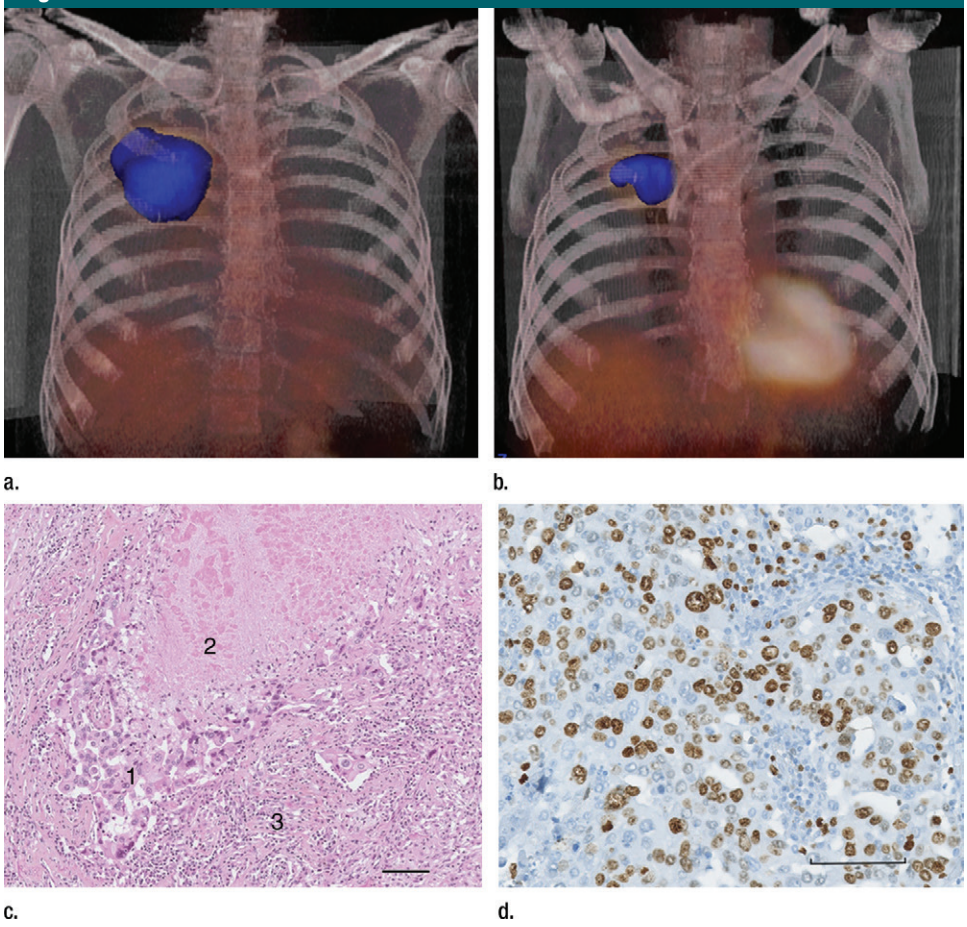

Figure 3: Images in a patient with an adenocarcinoma stage IIIA (T3N1, primary TV in blue). This case illustrates a mismatch between high decrease in TV and total lesion glycolysis and an increase in SUV_{max}. FDG PET was performed **(a)** before and **(b)** after three cycles of induction chemotherapy. SUV_{max}, TV, and total lesion glycolysis ratios were respectively 1.25, 0.2, and 0.2. **(c)** Histologic analysis of the entire resected specimen showed 30% of residual tumor cells (hematoxylin-eosin stain; scale bar: 100 μm; residual tumor cells *[1],* necrosis *[2],* and inflammatory cells *[3]*), **(d)** whereas proliferative index Ki-67 was estimated at 80% (immunohistochemical stain).

histologic responders than in incomplete responders (11,13,30). On the other hand, several studies indicated that FDG uptake does not reliably predict pathologic response after induction treatment (14). Our results showed that postinduction SUVs were positively correlated with Ki-67, but not with the residual viable tumor. In addition, postinduction SUV should be interpreted with caution because they can be caused by macrophage infiltration and not viable tumor tissue (15). We did not find any correlation between posttreatment SUVs and inflammatory infiltrate or the presence of foamy macrophages. This discrepancy can be explained by the use of chemotherapy alone as an induction treatment in our study, whereas radiation therapy combined with chemotherapy could have contributed to a more intense inflammatory response (15). Furthermore, other factors, such as hypoxia marker (ie, HIF-1 alpha) can contribute to the tumor uptake (31). Postinduction SUVs were also positively correlated with the presence of necrosis in this study. One explanation is that hypoxia can cause necrosis, but this is also a factor that contributes to the tumor uptake. Furthermore, the fact that larger tumors presented a higher amount of necrosis and a higher uptake than smaller tumors can also explain the link between SUV and necrosis. Finally, the time delay between PET imaging and surgery cannot exclude the presence of residual hypoxic, glucose-consuming cells at the time of PET acquisition that became areas of necrosis at the time of surgery.

Several limitations should be mentioned. First, this study included a small number of patients. Nevertheless, our population was homogeneous and included only patients with stage III disease who all received platinum-based induction chemotherapy. The

low number of patients prevented us from defining potential parameter cutoffs. Further larger prospective studies are needed to confirm our results and define relevant cutoffs. In addition, the small number of patients decreased the statistical power of the analyses when the correlation coefficients were less than 0.5, especially regarding the correlations between SUV_{max} or CT diameter ratios with the amount of residual tumor cells. However, the results of the stepwise analysis suggest that our conclusions were robust, despite the low number of patients. Second, the time to surgery varied from patient to patient, from 3.4 weeks to 11.8 weeks, based on the assumption of ongoing histopathologic changes between the end of chemotherapy and tumor removal. However, the variable time to surgery did not correlate with any of the imaging parameters and did not have a statistically significant effect on the results of the multivariate models. Finally, metabolic volume of pathologic lymph nodes was not taken into account because the delineation was hampered by the mediastinal background activity.

Although it requires further validation, prospective histopathologic estimation of the quantity of residual tumor cells appears to be an accurate prognostic factor in NSCLC treated with induction chemotherapy. Conversely, necrosis alone is not a good marker of response to treatment because it can be replaced by elastosic or scar tissue. The use of fibrous tissue to evaluate response is also problematic because it is difficult to distinguish between treatment-related fibrosis and fibrosis that is not related to treatment. To enhance prognostic accuracy of residual tumor cells, it could be interesting to refine the evaluation of cell viability and the importance of cytologic changes observed in some tumors after induction (5).

In conclusion, TV and total lesion glycolysis ratios helped predict residual viable tumor to preoperative chemotherapy in locally advanced NSCLC. SUV ratios were correlated with proliferative activity of the tumor. Therefore, a combination of metabolic and volumetric indices might be of interest to characterize the histologic response after chemotherapy in NSCLC.

Disclosures of Conflicts of Interest: M.S. No relevant conflicts of interest to disclose. **J.C.** No relevant conflicts of interest to disclose. **C.P.** No relevant conflicts of interest to disclose. **K.C.** No relevant conflicts of interest to disclose. **F.O.** No relevant conflicts of interest to disclose. **E.M.** No relevant conflicts of interest to disclose. **V.E.** No relevant conflicts of interest to disclose. **J.F.M.** No relevant conflicts of interest to disclose. **I.B.** No relevant conflicts of interest to disclose.

References

1. Boyle P, Ferlay J. Cancer incidence and mortality in Europe, 2004. Ann Oncol 2005;16(3):481–488.
2. Berghmans T, Paesmans M, Sculier JP. Prognostic factors in stage III non-small cell lung cancer: a review of conventional, metabolic and new biological variables. Ther Adv Med Oncol 2011;3(3):127–138.
3. Farray D, Mirkovic N, Albain KS. Multimodality therapy for stage III non-small-cell lung cancer. J Clin Oncol 2005;23(14):3257–3269.
4. Depierre A, Milleron B, Moro-Sibilot D, et al. Preoperative chemotherapy followed by surgery compared with primary surgery in resectable stage I (except T1N0), II, and IIIa non-small-cell lung cancer. J Clin Oncol 2002;20(1):247–253.
5. Junker K, Langner K, Klinke F, Bosse U, Thomas M. Grading of tumor regression in non-small cell lung cancer : morphology and prognosis. Chest 2001;120(5):1584–1591.
6. Junker K, Thomas M, Schulmann K, Klinke F, Bosse U, Müller KM. Tumour regression in non-small-cell lung cancer following neoadjuvant therapy. Histological assessment. J Cancer Res Clin Oncol 1997;123(9):469–477.
7. Pataer A, Kalhor N, Correa AM, et al. Histopathologic response criteria predict survival of patients with resected lung cancer after neoadjuvant chemotherapy. J Thorac Oncol 2012;7(5):825–832.
8. Shankar LK, Hoffman JM, Bacharach S, et al. Consensus recommendations for the use of 18F-FDG PET as an indicator of therapeutic response in patients in National Cancer Institute Trials. J Nucl Med 2006;47(6):1059–1066.
9. Young H, Baum R, Cremerius U, et al. Measurement of clinical and subclinical tumour response using [18F]-fluorodeoxyglucose and positron emission tomography: review and 1999 EORTC recommendations. European Organization for Research and Treatment of Cancer (EORTC) PET Study Group. Eur J Cancer 1999;35(13):1773–1782.
10. Akhurst T, Downey RJ, Ginsberg MS, et al. An initial experience with FDG-PET in the imaging of residual disease after induction therapy for lung cancer. Ann Thorac Surg 2002;73(1):259–264; discussion 264–266.
11. Cerfolio RJ, Bryant AS, Winokur TS, Ohja B, Bartolucci AA. Repeat FDG-PET after neoadjuvant therapy is a predictor of pathologic response in patients with non-small cell lung cancer. Ann Thorac Surg 2004;78(6):1903–1909; discussion 1909.
12. Choi NC, Fischman AJ, Niemierko A, et al. Dose-response relationship between probability of pathologic tumor control and glucose metabolic rate measured with FDG PET after preoperative chemoradiotherapy in locally advanced non-small-cell lung cancer. Int J Radiat Oncol Biol Phys 2002;54(4):1024–1035.
13. Ryu JS, Choi NC, Fischman AJ, Lynch TJ, Mathisen DJ. FDG-PET in staging and restaging non-small cell lung cancer after neoadjuvant chemoradiotherapy: correlation with histopathology. Lung Cancer 2002;35(2):179–187.
14. Port JL, Kent MS, Korst RJ, Keresztes R, Levin MA, Altorki NK. Positron emission tomography scanning poorly predicts response to preoperative chemotherapy in non-small cell lung cancer. Ann Thorac Surg 2004;77(1):254–259; discussion 259.
15. Poettgen C, Theegarten D, Eberhardt W, et al. Correlation of PET/CT findings and histopathology after neoadjuvant therapy in non-small cell lung cancer. Oncology 2007;73(5-6):316–323.
16. Larson SM, Erdi Y, Akhurst T, et al. Tumor treatment response based on visual and quantitative changes in global tumor glycolysis using PET-FDG imaging. The visual response score and the change in total lesion glycolysis. Clin Positron Imaging 1999;2(3):159–171.
17. Soussan M, Chouahnia K, Maisonobe JA, et al. Prognostic implications of volume-based measurements on FDG PET/CT in stage III non-small-cell lung cancer after induction chemotherapy. Eur J Nucl Med Mol Imaging 2013;40(5):668–676.
18. Boffa DJ, Detterbeck FC, Smith EJ, et al. Should the 7th edition of the lung cancer stage classification system change treatment algorithms in non-small cell lung cancer? J Thorac Oncol 2010;5(11):1779–1783.

19. Kawai T, Suzuki M, Kono S, et al. Proliferating cell nuclear antigen and Ki-67 in lung carcinoma. Correlation with DNA flow cytometric analysis. Cancer 1994;74(9):2468–2475.

20. Surti S, Kuhn A, Werner ME, Perkins AE, Kolthammer J, Karp JS. Performance of Philips Gemini TF PET/CT scanner with special consideration for its time-of-flight imaging capabilities. J Nucl Med 2007;48(3):471–480.

21. El Fakhri G, Surti S, Trott CM, Scheuermann J, Karp JS. Improvement in lesion detection with whole-body oncologic time-of-flight PET. J Nucl Med 2011;52(3):347–353.

22. Accorsi R, Adam LE, Werner ME, Karp JS. Optimization of a fully 3D single scatter simulation algorithm for 3D PET. Phys Med Biol 2004;49(12):2577–2598.

23. Eisenhauer EA, Therasse P, Bogaerts J, et al. New response evaluation criteria in solid tumours: revised RECIST guideline (version 1.1). Eur J Cancer 2009;45(2):228–247.

24. Marten K, Engelke C. Computer-aided detection and automated CT volumetry of pulmonary nodules. Eur Radiol 2007;17(4):888–901.

25. Tylski P, Stute S, Grotus N, et al. Comparative assessment of methods for estimating tumor volume and standardized uptake value in (18)F-FDG PET. J Nucl Med 2010;51(2):268–276.

26. Dooms C, van Baardwijk A, Verbeken E, et al. Association between 18F-fluoro-2-deoxy-D-glucose uptake values and tumor vitality: prognostic value of positron emission tomography in early-stage non-small cell lung cancer. J Thorac Oncol 2009;4(7):822–828.

27. Hatt M, Groheux D, Martineau A, et al. Comparison between 18F-FDG PET image-derived indices for early prediction of response to neoadjuvant chemotherapy in breast cancer. J Nucl Med 2013;54(3):341–349.

28. Moon SH, Cho SH, Park LC, et al. Metabolic response evaluated by 18F-FDG PET/CT as a potential screening tool in identifying a subgroup of patients with advanced non-small cell lung cancer for immediate maintenance therapy after first-line chemotherapy. Eur J Nucl Med Mol Imaging 2013;40(7):1005–1013.

29. Soret M, Bacharach SL, Buvat I. Partial-volume effect in PET tumor imaging. J Nucl Med 2007;48(6):932–945.

30. Yamamoto Y, Nishiyama Y, Monden T, et al. Correlation of FDG-PET findings with histopathology in the assessment of response to induction chemoradiotherapy in non-small cell lung cancer. Eur J Nucl Med Mol Imaging 2006;33(2):140–147.

31. van Baardwijk A, Dooms C, van Suylen RJ, et al. The maximum uptake of (18)F-deoxyglucose on positron emission tomography scan correlates with survival, hypoxia inducible factor-1alpha and GLUT-1 in non-small cell lung cancer. Eur J Cancer 2007;43(9):1392–1398.